Effect of Nitriding Voltage on the Impact Load Fatigue and Fracture Toughness Behaviour of CoCrMo Alloy Nitrided Utilising a HIPIMS Discharge

SHUKLA, Krishnanand, PURANDARE, Yashodhan <http://orcid.org/0000-0002-7544-9027>, KHAN, Imran, EHIASARIAN, Arutiun <http://orcid.org/0000-0001-6080-3946> and HOVSEPIAN, Papken <http://orcid.org/0000-0002-1047-0407>

Effect of Nitriding Voltage on the Impact Load Fatigue and Fracture Toughness Behaviour of CoCrMo Alloy Nitrided Utilising a HIPIMS Discharge

Krishnanand Shukla[1], Yashodhan P. Purandare[1], Imran Khan[2], Arutiun. P. Ehiasarian[1], Papken. Eh. Hovsepian[1]

[1]National HIPIMS Technology Centre UK, Materials and Engineering Research Institute, Sheffield Hallam University, Sheffield, S1 1WB, UK.

[2]Zimmer-Biomet UK Limited, Dorcan Industrial Estate, Murdock Road, Swindon SN3 5HY, UK.

*** Corresponding author: kshukla488@gmail.com**

Abstract:

CoCrMo alloy specimens were plasma nitrided using a High Power Impulse Magnetron Sputtering (HIPIMS) discharge. In this work the effect of nitriding voltage (-700 V to -1100 V) on the microstructure, surface hardness, impact load fatigue resistance and fracture toughness (K_{Ic}) of the alloy has been investigated.

Results revealed that the specimens treated at lower nitriding voltages (-700 V and -900 V) develop a nitrided layer consisting a mixture of Co_4N+$Co_{2-3}N$ phases. As the nitriding voltage increased (-1000 V and -1100 V), this transformed into a thick layer consisting mainly of $Co_{2-3}N$ with a minor contribution from CrN/Cr_2N phases. Accordingly, surface hardness tests after nitriding showed a significant improvement in hardness value (H= 23 GPa) as compared to the untreated specimen, (H= 7.9 GPa). The impact resistance of the alloy also increased with the nitriding voltage. Impact crater profiling of the specimens subjected to impact load tests showed that the depth of the crater decreased significantly,

especially at higher nitriding voltages. At the end of the impact load test (one million impacts), the crater depth for an untreated alloy (12.78 μm) was found to be twice to the crater depth measured for the specimen nitrided at -1100 V (7.1 μm). Impact testing results indicate that the fatigue endurance limit of the CoCrMo alloy increased steadily and considerably with the increase of the nitriding voltage. HIPIMS plasma nitriding resulted in a layer material with improved plain strain fracture toughness (K_{Ic}), with higher values (K_{Ic}) = 1011 MPamm$^{1/2}$ (-700 V specimen) were calculated as compared to K_{Ic} = 908 MPamm$^{1/2}$ for the untreated specimens. Critical material parameter ratios such as H/E (elastic index or elastic strain to failure) and H^3/E^2 (plastic index) of the nitrided layers were calculated using surface hardness (H) and elastic modulus (E) values obtained with the help of nanoindentation tests. Systematic improvement in the values of H/E and H^3/E^2 ratios calculated for all nitrided specimens validated the increase in fracture toughness and impact load fatigue resistance of the nitrided specimens as compared to the corresponding properties of the untreated CoCrMo base alloy.

Keywords: HIPIMS Discharge; Nitriding; CoCrMo alloy; Fracture toughness; Impact Load Fatigue resistance.

1. Introduction:

CoCrMo alloy, also known as ASTM-F75, is widely used in the manufacturing of load-bearing prostheses such as hip and knee implants [1]. Addition of Mo (about 5-7 wt%) to CoCr alloy refines its grains and improves the mechanical properties, such as tensile strength [2, 3]. Whereas, the addition of chromium (Cr) at 28-30 wt % in the alloy matrix enhances it's corrosion resistance due to the formation of Cr oxides layers on the surface when exposed to a corrosive environment [2-6]. However, despite it's excellent corrosion resistance and tensile strength, this alloy suffers from poor wear resistance which minimises the lifetime of the implants [7].

In recent years, surface hardening techniques such as gas nitriding, plasma nitriding/ carburising [3, 8], Ion Implantation [9-11], boronisation [12], oxidising and very recently High Power Impulse Magnetron Sputtering (HIPIMS) nitriding [13] have been used to improve the wear resistance and surface hardness of these CoCrMo alloys. In general, a few micrometres thick nitrided layer on the surface improves wear resistance by one order of magnitude and significantly reduces the coefficient of friction [14, 15]. The improvement in surface hardness, tribological and fatigue properties have been attributed to the formation of a compound layer ($M_{2-3}N$; M=Fe, Co) followed by a diffusion layer (M_4N; M=Fe, Co) [14].

The phase composition of the compound layer has shown a strong dependence on the process temperature. It has been reported that when a nitriding treatment is carried out in the temperature range of 450 °C, the compound layer is based on CrN phase due to the precipitation of Cr. Tang et al., (2014) [16] found that nitriding of CoCrMo alloy at a process temperature of about 1000 ºC for one hour leads to the formation of Cr_2N, whereas at 800 °C no nitride formation was observed. Wang et al., (2010) [2] mentioned that nitriding at temperatures higher than 700 °C leads to the formation of a nitrided layer comprising of a mixture of CrN and Cr_2N. They also reported that an increase in process temperature

conglomerates the surface material to form nanoparticles which leads to a rise in the surface roughness (R_a) value.

On the other hand, few researchers had reported the layers to be free of Cr based phases when the process temperature was below 450 °C. Pichon et al., (2010) found that temperature around 400 °C promotes the formation of metastable γN phase without any Cr based compound layer [17]. Wei et al., (2004) demonstrated that CoCrMo alloy nitrided at 400 °C using high-intensity ion plasma nitriding (HIIPN) showed a nitrided layer (γ_N) thickness of about 0.5 µm. However, the rise in temperature resulted in a dramatic increase in layer thickness and composition from 6.5 µm at 500 °C (Cr_2N and parent ε phase) to 23.6 µm at 700 °C ($CrN+Cr_2N$ and parent phases), with an increase in R_a value [11, 18]. Bazzoni et al., (2013) showed that the formation of a 4 to 5 µm thick compound layer (γ_N at 350 °C and γ_N+Cr_2N at 450 °C) improves the wear resistance and lowers the friction coefficient compared to those of the untreated specimens [19]. Bayak et al., (2010) have reported a decrease in the fatigue limit of the CoCrMo alloy due to nitriding [20]. Literature on the temperature (and hence energy availabe for diffusion), phase formation and changes in the mechanical properties, especially wear resistance after nitriding can be found, however, to the best of our knowledge, an extensive study on the fatigue and fracture toughness behaviour of plasma nitrided CoCrMo alloys that has never been reported.

HIPIMS technology is a recent development in the field of DC magnetron sputtering technique. HIPIMS utilises transient impulse (short pulses) glow discharge with very high power and current densities which results in the generation of a dense and energetic plasma, rich in both, reactive gas ions and metal ions (if employed for coating) [21]. Thus, when utilised for nitriding, the HIPIMS discharge is rich in activated atomic nitrogen (N^+) and diatomic nitrogen ions (N_2^+) compared to conventional plasma [22], where plasma composition is mainly dominated by diatomic N_2^+ [22]. This facilitates higher diffusion rates

and in general a rapid nitriding rate, however at lower temperatures than conventional nitriding. In the previous studies, the authors had demonstrated the use of HIPIMS discharge for plasma nitriding of CoCrMo alloys [13]. It was found that the microstructure was sensitive to the nitriding voltage (-700 V to -1100 V) applied to the specimens and not to the temperature as it was fixed at 400 °C. However, detailed investigation on the relationship between the properties and microstructure of these layers was not reported. In the current work, mechanical properties such as nanohardness, toughness, K_{Ic} and impact fatigue resistance of these nitrided layers have been evaluated. A rational relationship between the performance and the microstructure has been presented.

2. Experimental Details:

2.1 Materials and Method:

Disc-shaped specimens of 25 mm diameter and 6 mm thickness, made from CoCrMo alloy (ASTM F75) were prepared up to mirror-like appearance (R_a= <15 nm) by using the standard metallographic procedure. The chemical composition of ASTM F75 can be found elsewhere [1]. Before loading into the chamber, samples were cleaned in an automated industrial-sized cleaning line containing various water baths based on industrial detergents such as alkali solutions along with ultrasonic agitation to remove organic contaminants from the surface. Following this cleaning stage, the samples were rinsed by deionised water and vacuum dried at a temperature of 90 °C. Plasma nitriding using HIPIMS discharge was carried out in an industrial-sized PVD machine (Hauzer techno Coating 1000-4, The Netherlands) equipped with two HIPIMS (Hüttinger Elektronik Sp. z o.o., Warsaw, Poland) and two DC power supplies and a dedicated bias power supply (Hüttinger Elektronik Sp. z o.o., Warsaw, Poland) with an arc suppression unit [23]. Samples were mounted on a rotating table in the middle of the chamber and subjected to three-fold rotation, which allowed for uniform exposure of the

surface to the ion bombarding flux. The nitriding voltages were varied between -700 V to -1100 V in order to investigate a wide range of bombarding energies. The temperature was precisely monitored with specially designed electronically isolated thermocouples mounted on the substrate table in the vacuum chamber allowing direct temperature measurement during the process. The system is equipped with high precision gas flow controllers operating in the range of 0-500 sccm to control the gas flow of nitrogen-hydrogen mixture (N_2:H_2) and argon (Ar). Plasma emission monitoring (Gencoa SpeedFlo) was used to control the reactive gas flow during the process. The process temprature and pressure were set constant at 400 °C and 8.3×10^{-3} mbar respectively for all the experiments. Detailed information on the plasma nitriding processes using HIPIMS discharge can be found in the previous publication [13].

2.2 Characterisation technique:

The mechanical properties of HIPIMS nitrided specimens were characterised using various advanced analytical techniques.

- Plan and cross-sectional scanning electron microscopy (CS-SEM) studies were carried out using FEI Quanta 650 3D DualBeam FIB FEG-SEM equipped with a secondary electron detector (SE). The Focused Ion Beam (FIB) capability available in the SEM was also used for milling in order to image the areas of interest. Prier to imaging, the manually prepared cross-section surfaces were polished using 1 µm diamond paste and etched for 16 seconds using Marble's reagent ($HCL+H_2O_2$ etchant) to reveal the nitrided layer in the SEM studies.
- CSM-Anton Paar nanohardness tester was used to obtain elastic modulus and nanohardness values of all the specimens using a maximum load of 5 mN.
- CemeCon impact load tester was used to evaluate the impact load fatigue behaviour of the nitrided and untreated specimens under dynamic loading conditions. The counterpart

was tungsten carbide (WC) ball of 6 mm diameter. A fixed normal load of 500 N was applied during all tests.

- Impact craters were profiled using a profilometer (DEKTAK 150 STYLUS) with a resolution of 33 nm.
- The fracture toughness values of all specimens were calculated using the formula proposed in [24-26].

$$K_{IC} = \delta \left(\frac{E}{H}\right)^{0.5} \left(\frac{P}{c^{3/2}}\right)$$

Where, E (Nmm^{-2}) is the elastic modulus of nitrided layer, H (Nmm^{-2}) is the Vickers microhardness, P (N) is the fixed applied load (50 kgf), and c (mm) is the average radial crack length obtained from the indentation impression using a SEM.

3. Results and Discussion:

3.1 Microstructure Analysis

Figure 1 shows the SEM cross-sectional view of the specimens nitrided with nitriding voltages of -700 V to -1100 V. It was clear from the above images that the nitrided layer thickness increased proportionally with an increase in the nitriding voltage. Out of all the treated specimens, the thickest nitrided layer of around 5 µm was observed for the specimen nitrided with -1100 V. The layer thickness measured for the specimen plasma nitrided with -700 V, -900 V and -1000 V was found to be around 1 µm, 1.6 µm and 3.62 µm respectively. Apart from the thickness, the variation of the nitriding voltage impacted significantly on the phase composition of the layers formed. Specimens nitrided with -700 V and -900 V were found to have a mixture of both S-phase (also known as white diffusion layer (Co_4N) and a grey compound layer made up of $Co_{2\text{-}3}N$. The diffusion layer thickness decreased with an increase in nitriding voltage. At the higher nitriding voltages of -1000 V and -1100 V, the

diffusion layer was difficult to resolve and was not clearly visible. Apart from the $Co_{2-3}N$ compound layer (Co_4N+$Co_{2-3}N$), presence of CrN and Cr_2N was also detected. A detailed investigation of elemental composition and texture of these nitrided layers has been presented in a previous publication [13]. The XRD data (not presented here) for these specimens confirmed the presence of both Co_4N and $Co_{2-3}N$, also termed as expanded austenite phase $\gamma_N(111)$ and $\gamma_N(200)$. Interestingly, as the nitriding voltage increased from -700 V to -1100 V, the texture of the nitrided layers also changed from a predominant (200) orientation to a mixture of both (111) and (200) orientations. Table 1 summarises these results and has been included in this paper for reference.

3.2 Impact Fatigue Analysis:

In order to evaluate the effectiveness of the nitriding process, the impact resistance response of the specimens was tested using a dedicated impact load tester. In this test, a fixed normal load of 500 N was applied, whereas the number of total impacts was varied to better trace the impact size progression with time. For each specimen, the test was interrupted initially after 250 impacts and then progressed to 1.10^6 impacts. The craters were depth profiled using a Dektak Stylus profilometer by conducting a linear scan across the crater after each stage.. The values of the initial crater depth (d_i) after 250 impacts and final, crater depth (d_f) after 1.10^6 impacts are summarised in Table 2.

From Table 2, it is apparent that the deepest crater, after both, 250 and 1.10^6 impacts were observed for the untreated alloy, which was around 12.73 µm. The HIPIMS plasma nitrided specimens showed a better response against both initial and final impacts compared to the untreated specimen. In the case of the specimen nitrided at -1100 V, the values of d_i= 7.16 µm and d_f = 7.23 µm observed respectively were the lowest values amongst the specimens investigated. The steady decrease in both d_i and d_f values with an increasing nitriding voltage

demonstrated that nitriding significantly improved the impact load resistance of the surface of the CoCrMo alloy.

Figure 2(a), shows the crater surface morphology of the untreated alloy after one million impacts. The impact area can be divided into two different zones; Zone 1: the area around the periphery of the crater and Zone 2: middle of the crater. Zone-1 distinctively showed an accumulation of wear debris displaced from the impact crater. High magnification SEM image of zone-1 revealed that the surface deformed via a continuous formation of shear bands (parallel to each other). These bands appeared to criss-cross each other, as shown in figure 2(c). Also, cracks near the bottom of these shear bands were detected in the *FIB-CS* ((Focused Ion Beam-cross section), figure 2b). On the other hand, in zone 2, the crater was found with islands of metal oxides adhered to the base metal which had a thickness of about 0.7 µm confirmed via *FIB-CS* and *EDS* (Energy Dispersive Spectroscopy) elemental mapping (figure 2d and figure 4 respectively). Despite the high number of impacts of one million, no evidence of any crack formation in the underneath material was observed in this zone. It is believed that plastic deformation, oxidation of the surface followed by subsequent removal of these oxides due to cracking seemed to be the main mechanism of crater formation.

The impact crater surface analysis of specimen nitrided at -700 V to -1100 V revealed that in this voltage range the diameter (and consequently the depth of the craters) reduced with higher rate from 575 µm for -700 V to 518 µm for -1100 V as shown in figure 3 and Table 2. However, in all cases the increase in nitriding voltage resulted in an improvement in impact resistance of the nitrided layer which can be attributed to the synergistic effect of the changes in thickness, surface texture, microstructure, phase composition and hardness on the increase in the shock-absorbing capacity of the nitrided layer.

EDS elemental mapping was performed to better understand the chemistry of the various compounds formed on the surface of the craters. The colour coded EDS elemental maps are shown in figure 4. In general, brighter the colour (assigned to an element) in the map, higher is the concentration of that element. In addition to the main elements such as Cobalt (Co), Chromium (Cr) and Molybdenum (Mo) of the alloy and Nitrogen (N) due to the treatment, the elements Oxygen (O) and Tungsten (W) were also investigated to reveal the effect of the surrounding environment (impact due to oxidation) and potential material transfer due to the impact wear of the WC counterpart. The analyses showed that the crater surface of the specimen nitrided at -700V was fully covered with an oxide layer. The amount of oxide formation reduced gradually as the voltage increased from -900 V to -1100 V, as shown in figure 4 and FIB-CS images, figure 5(b-d). One possible reason for this behaviour could be the increase in the amount of CrN/Cr_2N in the nitrided layers. In concurrence, the material transfer from the WC counterpart also increased. This behaviour can be attributed to the overall increased hardness and toughness of the nitrided layer.

The sub-surface microstructure of the material beneath the impact craters of the nitrided specimens was investigated by FIB-SEM analyses, figure 5. In the case of specimens nitrided at -1000 V and -1100 V (figure 5c-d), fatigue cracks within the base metal beneath the nitrided layer were observed. Interestingly, no such cracks were observed in the case of -700 V and -900 V specimens. In this study, the nitrided layers formed at -900 V showed the best combination of oxidation resistance and impact energy damping capability. Whereas, in the case of -1000 V to -1100 V, impact energy absorbed by nitrided layers has transferred to the base metal resulting in crack formation.

An important correlation between the plasticity index, H^3/E^2 and impact response was presented by Chen and co-workers in 2011 where they found that the specimen with higher plasticity index, (H^3/E^2) was found to have a better response against nano impact [27].

Table 1 summarises the data regarding the surface nanohardness (H), elastic modulus (E), texture coefficient (T*), elastic index (H/E) and plasticity index (H^3/E^2). It can be stated that whilst the hardness values of the nitrided layers produced at different nitriding voltages were found approximately similar, the E values showed an increase from 265.5 GPa for -700 V to 343.1 GPa for -1100 V. This is reflected by the values of the plasticity index where the maximum plasticity index, H^3/E^2 (H= 22 GPa and E= 265.5 GPa) value of 0.15 was observed for specimen nitrided at -700 V whereas it decreased to 0.10 (H= 23 GPa and E= 343.1 GPa) for specimen nitrided at -1100 V. Hence specimens nitrided with -700 V and -900 V demonstrated the best impact energy damping capability therefore resulting in excellent resistance against impact fatigue cracking, even though the nitrided layer thickness was much lower as compared to the specimens treated at -1000 V and -1100 V. It is believed that the impact energy was transferred from nitrided layer to the base metal, thereby leading to an increase in the fatigue crack density (within and beneath the compound layer). Thus impact test results suggest that -900 V, despite the thinner layer, shows the best combination of high oxidation resistance and high value of the plasticity index H^3/E^2.

3.3 Fracture Toughness (K_{Ic}):

To evaluate the fracture toughness value K_{Ic} of the relatively thin nitrided layer, an alternative method based on vickers indentation was used on HIPIMS nitrided and the untreated alloys [26-30]. In this indentation based method, the contact pressure is independent of the indentation size (IDS) and the quality of the indentation is evaluated in terms of plastic deformation and crack propagation from the edges and corners of the residual indentation impression. A STRUERS microhardness tester equipped with a vickers indenter (pyramidal shape) was used to make indentations. A fixed and excesivelly high penetration load of 50 kgf was applied irrespective of the nitrided layer thickness in order to promote crack initiation.

Figure 6 shows the calculated K_{Ic} value for the untreated and the nitrided specimens at different nitriding voltages. K_{Ic} value for the untreated specimen was around 906.9 MPamm$^{1/2}$ a relatively high value as expected for the softer base material, (Table 1). The highest K_{Ic} value of 1011.7 MPamm$^{1/2}$ was found for the -700 V specimen. A further increase in the nitriding voltage (-900 V) deteriorated the K_{Ic} value to 872.9 MPamm$^{1/2}$. However this value increased further as the nitriding voltage increased from -900 V to -1100 V, as shown in figure 6. The change in K_{Ic} value could be linked to the change in the texture of the compound layer [31]. The texture analyses of the specimen nitrided with -700 V showed that the predominant crystallographic orientation of the compound layer was (200). Whereas, at higher nitriding voltage from -900 V to -1100, the compound layer developed a mixed texture of (111) and (200). As the volume fraction of (200) texture increased from 56.42 % (-900 V) to 72 % (-1100 V), the fracture toughness value showed an increment accordingly.

Investigation of the surface morphology of the impression after indentation is also essential in order to evaluate the resistance of the nitrided alloy against cracking. In the vickers indentation method, usually, two kinds of crack modes namely Palmquist and radial cracking along the edges of the indenter, can be observed [29]. As per the formula, K_{Ic} is inversely proportional to the crack length formed along the edges of the indentation after unloading. Figure 7(a-c) shows the indentation impression on the surface of the untreated specimen for a fixed normal load of 50 kgf. No evidence of any types of cracks along the edges of the square impression due to a fracture was evident in the SEM studies. This suggested that the untreated alloy had high resistance against cracking as expected for a lower hardness and high plasticity material. However, high magnification SEM analysis of the indent showed shear cracking along the diagonals of the impression (figure 7b). Formations of such crack can be attributed to the manufacturing defects (micro-voids) and the associated localised strain around these. Further analysis of the area around the indentations showed that the

surface deformed plastically during the loading-unloading cycle, which was also made evident due to the presence of shear bands, [32] around the indentation (figure 7c).

Figure 8(a-c) shows the indentation made on the specimen nitrided at -700 V. In this case, the area around the square edges and corresponding corners of the impression were found crack free which indicates a good fracture toughness of the nitrided layer. However, further detailed surface analyses revealed interesting features of the deformation behaviour of such layers. For example, shear cracks were found in the areas near to the intersection of the diagonals (figure 8b) and very adjacent to the diagonals formed due to the point load concentration and high strain rates. Figure 8c shows the area where the diagonals meet at one of the corners of the square impression. In this image, shear bands along with the cracks and the surface texture of the nitrided surface were prominantly evident.

For specimens at higher nitriding voltages of -900 V, -1000 V and -1100 V, both Palmquist and radial mean type cracks were detected. Most of these cracks had their origin and extinction within the faces of the impressions, which followed the direction of loading. For specimens nitrided with -900 V, initiation and propagation of these cracks (Palmquist and radial) can be seen in figure 9(a-d). They were predominantly present around the boundary of the square impression (figure 9(a-b)). Similar to -700 V specimen, the cracks within the centre of impression (figure 9c) were found, but with higher density. Figure 9(d) shows a high magnification image of the radial cracks near the edges of the square. Apart from these cracks, shear bands which were further forced away from the indentation were also found (figure 9a). It is considered that hemispherical plastic zone (or semi-circular plastic zone) and radial stresses are responsible for the formation of these primary shear bands during the indentation [33-35].

Figures 10(a-c)-11(a-c) exhibit the impression after indentation on the specimens treated at -1000 V and -1100 V respectively. It can be concluded from above images that as nitriding voltage increased from -1000 V to -1100 V, the number of radial cracks along the edges and around the corners decreased while the cracks within the impression (pyramidal faces) increased in population and became wider and symmetrical.

The difference in the fracture behaviour of the layers nitrided at lower voltages (-700 V, - 900 V) as compared to those produced at higher nitriding voltagees, (- 1000 V, - 1100 V) can be explained based on the specific hardness to Young's modulus ratios. A layer with a high value of H^3/E^2 ratio designates the surface to be of a high toughness with reduced plastic deformation. Also, a high H/E ratio defines the crack density, which means specimens with a high H/E ratio will have less crack population than the specimen with the lower value of H/E [38]. In our work, we also found similar trends where H/E ratio decreased with an increase in nitriding voltage. Hence in this work, -700 V specimen was found to be having the best K_{Ic} value since it had the least crack population (Palmquist and Radial) despite being the thinnest of all nitrided layers. However, when compared to the untreated alloy properties the HIPIMS plasma nitrided layers consistently showed a significant hardness increase and significant increase of the H^3/E^2 values in some cases up to almost two orders of magnitude, (see Table 1) and therefore enhanced fracture toughness.

It has been widely reported that state of the art nitriding improves hardness, but results in surface embrittlement [36, 37]. In our case, similar hardness increase was observed associated with the changes in the phase composition of the nitrided layer. However, in this work, we found that as the nitriding voltage increased the number of the shear band (after impact load tests) decreased which evidenced an improvement in the fracture toughness of the treated layers. In addition to the above made argument regarding increased K_{Ic} values, it can be speculated that this unusual behaviour is also due to structure specific properties

namely nitrided layer density. This is expeted to be much higher thanks to the high energy ion bombardment, (ion peening) achieved with utilisation of the highly ionised HIPIMS discharge.

4. Conclusions:

1. CoCrMo alloys were plasma nitrided at various nitriding voltages (-700 V to -1100 V) using HIPIMS discharge in an industrial-sized PVD machine. The SEM cross-section analysis revealed that the thickness of the nitrided layer is proportionate to the nitriding voltage. At the higher nitriding voltages of -1100 V, the thickness of the nitrided layer reached 5µm.
2. The nanohardness test showed that high hardness values of upto 23 GPa (-1100 V) could be achieved with HIPIMS nitriding, which was a significant improvement as compared to the untreated specimen, 7.9 GPa.
3. HIPIMS nitriding significantly enhanced the impact load behaviour of the base CoCrMo alloy. After one million impacts at 500 N normal load the crater depth on the treated specimens steadily reduced with nitriding voltage from 11.98 µm for nitriding voltage of -700V to 7.23 µm for voltage of -1100 V. In comparison the untreated substrate formed larger crater with depth of 12.78 µm under the same test conditions.
4. Systematic improvement in the values of H/E and H^3/E^2 ratios calculated for all HIPIMS nitrided specimens validated the increase in fracture toughness, (K_{Ic} value) and impact load fatigue resistance of the nitrided specimens as compared to the corresponding properties of the untreated CoCrMo base alloy. The best results were achieved (no crack formation in the nitrided layer and the base material beneath the impact load crater) with a nitriding voltage of -900 V.

5. Acknowledgement

The authors would like to acknowledge *Zimmer-Biomet, UK* for providing financial support for this research. We would also like to thank Mr. Gary Robinson and Mr. Paul Allender for technical assistance.

6. References

[1] A. F75-18, Standard Specification for Cobalt-28 Chromium-6 Molybdenum Alloy Castings and Casting Alloy for Surgical Implants (UNS R30075), ASTM Int. PA (2018). https://doi.org/10.1520/F0075-18.

[2] Q. Wang, L. Zhang, J. Dong, Effects of Plasma Nitriding on Microstructure and Tribological Properties of CoCrMo Alloy Implant Materials, J. Bionic Eng. 7 (2010) 337–344. https://doi.org/10.1016/S1672-6529(10)60265-X.

[3] A. Çelik, Ö. Bayrak, A. Alsaran, I. Kaymaz, A.F. Yetim, Effects of plasma nitriding on mechanical and tribological properties of CoCrMo alloy, Surf. Coatings Technol. 202 (2008) 2433–2438. https://doi.org/10.1016/j.surfcoat.2007.08.030.

[4] P.E. Sinnett-Jones, J.A. Wharton, R.J.K. Wood, Micro-abrasion-corrosion of a CoCrMo alloy in simulated artificial hip joint environments, Wear. 259 (2005) 898–909. https://doi.org/10.1016/j.wear.2005.02.045.

[5] G. Bellfontaine, The Corrosion of CoCrMo Alloys for Biomedical Applications, The University of Birmingham, 2010. papers2://publication/uuid/D3611780-AA0A-4FAA-8CC8-4651D8B48A2B.

[6] X. Luo, X. Li, Y. Sun, H. Dong, Tribocorrosion behavior of S-phase surface engineered medical grade Co–Cr alloy, Wear. 302 (2013) 1615–1623. https://doi.org/10.1016/j.wear.2013.01.023.

[7] D.C. Ba, L. Xu, Q. Wang, Effects of plasma nitriding ion beam flux density and time on the properties of CoCrMo alloy, Vacuum. 119 (2015) 214–222. https://doi.org/10.1016/j.vacuum.2015.05.032.

[8] H.D. Ran Liu, Xiaoying Li □, Xiao Hu, Surface modification of a medical grade Co-Cr-Mo alloy by low-temperature plasma surface alloying with nitrogen and carbon, Surf. Coatings Technol. J. 232 (2013) 906–911. https://doi.org/10.1016/j.surfcoat.2013.06.122

[9] J. Lutz, S. Mändl, Effect of ion energy and chemistry on layer growth processes during nitriding of CoCr alloys, Nucl. Instruments Methods Phys. Res. Sect. B Beam Interact. with Mater. Atoms. 267 (2009) 1522–1525.https://doi.org/10.1016/j.nimb.2009.01.083.

[10] J. Lutz, C. Díaz, J.A. García, C. Blawert, S. Mändl, Corrosion behaviour of medical CoCr alloy after nitrogen plasma immersion ion implantation, Surf. Coatings Technol. 205 (2011) 3043–3049. https://doi.org/10.1016/j.surfcoat.2010.11.017.

[11] R. Wei, T. Booker, C. Rincon, J. Arps, High-intensity plasma ion nitriding of orthopedic materials: Part I. Tribological study, Surf. Coatings Technol. 186 (2004) 305–313. https://doi.org/10.1016/J.SURFCOAT.2004.02.052.

[12] M. Alvarez-Vera, A. Juarez-Hernandez, C.E. Gonzalez-Rivera, R.D. Mercado-Solis, M.A.L. Hernandez-Rodriguez, Biotribological response of Co-Cr alloy with added boron under ball-on-disc tests, Wear. 301 (2013) 243–249. https://doi.org/10.1016/j.wear.2012.11.074.

[13] Krishnanand Shukla, Arunprabhu A. Sugumaran, Imran Khan, A. P. Ehiasarian and Papken Eh. Hovsepian, Low pressure plasma nitrided CoCrMo alloy utilising HIPIMS discharge for biomedical applications, Submitt. Publ. to J. Mech. Behav. Biomed. Mater. Revision completed (JMBBM_2020_70R1).

[14] E.J. Mittemeijer, Fundamentals of Nitriding and Nitrocarburizing, in: . Dossett and G.E.

Totten (Ed.), ASM Handb. Steel Heat Treat. Fundam. Process., 2013: pp. 619–646.

[15] D. Pye, Practical NITRIDING and Ferritic Nitrocarburizing, Pract. Nitriding Ferritic Nitrocarburizing. (2003). www.asminternational.org.

[16] N. Tang, Y. Li, Y. Koizumi, A. Chiba, Nitriding of Co-Cr-Mo alloy in nitrogen, Mater. Chem. Phys. 145 (2014) 350–356.https://doi.org/10.1016/j.matchemphys.2014.02.023.

[17] L. Pichon, S. Okur, O. Öztürk, J.P. Rivière, M. Drouet, CoCrMo alloy treated by floating potential plasma assisted nitriding and plasma based ion implantation: Influence of the hydrogen content and of the ion energy on the nitrogen incorporation, Surf. Coatings Technol. 204 (2010) 2913–2918. https://doi.org/10.1016/j.surfcoat.2010.01.050.

[18] B.R. Lanning, R. Wei, High intensity plasma ion nitriding of orthopedic materials. Part II. Microstructural analysis, Surf. Coatings Technol. 186 (2004) 314–319. https://doi.org/10.1016/j.surfcoat.2004.02.047.

[19] A. Bazzoni, S. Mischler, N. Espallargas, Tribocorrosion of Pulsed Plasma-Nitrided CoCrMo Implant Alloy, Tribol. Lett. 49 (2013) 157–167. https://doi.org/10.1007/s11249-012-0047-0.

[20] Ö. Bayrak, A.F. Yetim, A. Alsaran, A. Çelik, Fatigue life determination of plasma nitrided medical grade CoCrMo alloy, Fatigue Fract. Eng. Mater. Struct. 33 (2010) 303–309. https://doi.org/10.1111/j.1460-2695.2010.01442.x.

[21] A. P. Ehiasarian. Fundamentals and applications of HIPIMS. Plasma Surface Engineering Research and its Applications, 2008:35-85 ISBN:987-81-308-0257-2. Editor: Ronghua Wei. Research Signpost 37/661 (2), Fort P.O. Travandrum-695 023, Kerala, India.

[22] P. Hovsepian, G. Thompson. B. Lewis, A. Ehiasarian, and W.-D. Munz, Performance of High-Precision Knife Blades Treated by Plasma Nitriding and PVD Coating. SVC -

46th Annual Technical Conference Proceedings, San Francisco, CA, USA, May 2003.

[23] A. P. Ehiasarian, R. Tietema, R. Bugyi, A. Klimczak, D. Doerwald. A vacuum treatment apparatus a bias power supply and a method of operating a vacuum treatment apparatus. Pat. ZL 200780012990.9. 10.04. 2007.

[24] S. Zhang, D. Sun, Y. Fu, H. Du, Toughness measurement of thin films: a critical review, Surf. Coatings Technol. 198 (2005) 74–84. https://doi.org/10.1016/j.surfcoat.2004.10.021.

[25] F. Sergejev, Comparative study on indentation fracture toughness measurements of cermets and hardmetals, Euro PM 2006 - Powder Metall. Congr. Exhib. 1 (2006) 43–48.

[26] O. Al-Mana, M.S.J. Hashmi, B.S. Yilbas, Laser nitriding of titanium alloy and fracture toughness measurement of resulting surface, Adv. Mater. Res. 445 (2012) 615–620. https://doi.org/10.4028/www.scientific.net/AMR.445.615.

[27] J. Chen, H. Li, B.D. Beake, Load sensitivity in repetitive nano-impact testing of TiN and AlTiN coatings, Surf. Coatings Technol. 308 (2016) 289–297. https://doi.org/10.1016/j.surfcoat.2016.05.094.

[28] R. Documents, S. Factor, P.F. Toughness, C.P. Orientation, Standard Test Method for Linear-Elastic Plane-Strain Fracture Toughness K Ic of Metallic Materials, ASTM E399-20, (2010). https://doi.org/10.1520/E0399-09E02.2.

[29] Q. Yao, J. Sun, G. Zhang, W. Tong, H. Zhang, Enhanced toughness of nitrided layers formed on Ti-6Al-4V alloy via surface mechanical attrition pre-treatment, Vacuum. 142 (2017) 45–51. https://doi.org/10.1016/j.vacuum.2017.05.004.

[30] Q. Yao, J. Sun, Y. Fu, W. Tong, H. Zhang, An evaluation of a borided layer formed on Ti-6Al-4V alloy by means of SMAT and low-temperature boriding, Materials (Basel). 9 (2016). https://doi.org/10.3390/ma9120993.

[31] S. Suwas, R.K. Ray, Texture and Properties, in: Crystallogr. Texture Mater., Springer London, London, 2014: pp. 207–223. https://doi.org/10.1007/978-1-4471-6314-5_9.

[32] P. Manda, U. Chakkingal, A.K. Singh, Hardness characteristic and shear band formation in metastable β-titanium alloys, Mater. Charact. 96 (2014) 151–157. https://doi.org/10.1016/j.matchar.2014.07.027.

[33] S. Jana, U. Ramamurty, K. Chattopadhyay, Y. Kawamura, Subsurface deformation during Vickers indentation of bulk metallic glasses, Mater. Sci. Eng. A. 375–377 (2004) 1191–1195. https://doi.org/10.1016/j.msea.2003.10.068.

[34] M. Bagheripoor, R. Klassen, The effect of crystal anisotropy and pre-existing defects on the incipient plasticity of FCC single crystals during nanoindentation, Mech. Mater. 143 (2020) 103311. https://doi.org/10.1016/j.mechmat.2020.103311.

[35] Y. Kato, H. Yamazaki, S. Yoshida, J. Matsuoka, Effect of densification on crack initiation under Vickers indentation test, J. Non. Cryst. Solids. 356 (2010) 1768–1773. https://doi.org/10.1016/j.jnoncrysol.2010.07.015.

[36] Y. Sun, X. Li, T. Bell, Low temperature plasma carburising of austenitic stainless steels for improved wear and corrosion resistance, Surf. Eng. 15 (1999) 49–54. https://doi.org/10.1179/026708499322911647.

[37] T. Bell, Surface engineering of austenitic stainless steel, Surf. Eng. 18 (2002) 415–422. https://doi.org/10.1179/026708402225006268.

[38] X. Chen, Y. Du, Y.W. Chung, Commentary on using H/E and H3/E2 as proxies for fracture toughness of hard coatings, Thin Solid Films. 688 (2019) 0–1. https://doi.org/10.1016/j.tsf.2019.04.040.

Figure Captions

Figure 1: *CS-SEM* micrographs of specimens nitrided at (a) -700 V (b) -900 V (c) -1000 V and (d) -1100 V.

Figure 2: SEM micrographs (a) impact crater on the untreated alloy after 1.10^6 impacts, (b) FIB cross-section near shear bands (SB) (c) SB near the impact crater and (d) *FIB-CS* in zone 2 (middle) of the impact crater.

Figure 3: SEM micrographs of impact craters on the specimens nitrided at (a) -700 V (b) -900 V (c) -1000 V and (d) -1100 V after one million impacts.

Figure 4: Elemental mapping of impact craters on the untreated and plasma nitrided specimens at -700 V to -1100 V.

Figure 5: Sub-surface SEM micrographs of impact craters on the specimens nitrided at (a) -700 V (b) -900 V (c) -1000 V and (d) -1100 V.

Figure 6: Calculated fracture toughness (K_{Ic}) values of the untreated and specimens nitrided at -700 V to -1100 V.

Figure 7: SEM micrographs of (a) indentation on the untreated specimen (b) a high magnification image of the deformed area along the diagonal and (c) area near the edge and corner of the square impression.

Figure 8: SEM micrographs of (a) indent on specimens nitrided at -700 V (b) high magnification image of center of the impression and (c) one of the edges of the square impression.

Figure 9: SEM micrographs of (a) the indent on the surface of the specimen nitrided at -900 V (c) high magnification image of center of the impression and (d) one of the edges of the square impression.

Figure 10: SEM micrographs of (a) indents on the surface of the specimens nitrided at -1000 V (b) high magnification image of center of the impression and (c) one of the edges of the square impression.

Figure 11: SEM micrographs of (a) indents on the surface of the specimens nitrided at -1100 V (b) high magnification image of center of the impression and (c) one of the edges of the square.

Table Captions

Table 1: Texture (T*), nanohardness (H), Youngs modulus (E), calculated elastic and plastic index as well as nitrided layer thickness (L_D: diffusion thickness, L_C: compound layer thickness, and L_T: total layer thickness) of the untreated specimen and the nitrided specimens.

Table 2: Impact crater depth values of the untreated and the nitrided specimens after initial impacts (250) and final impact (one million impacts).

Figures

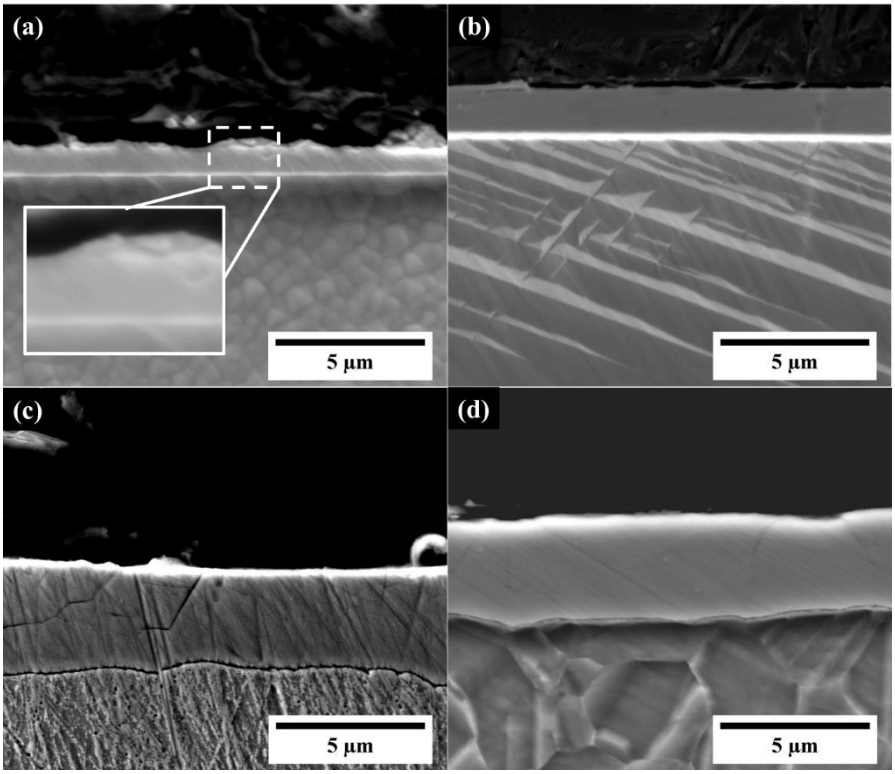

Figure 1

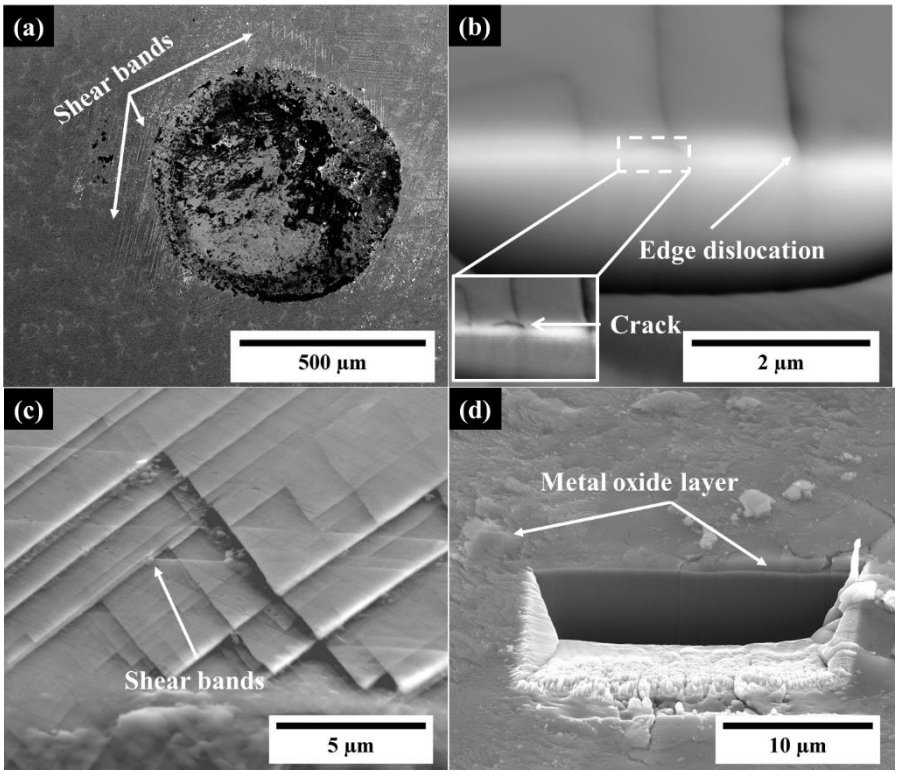

Figure 2

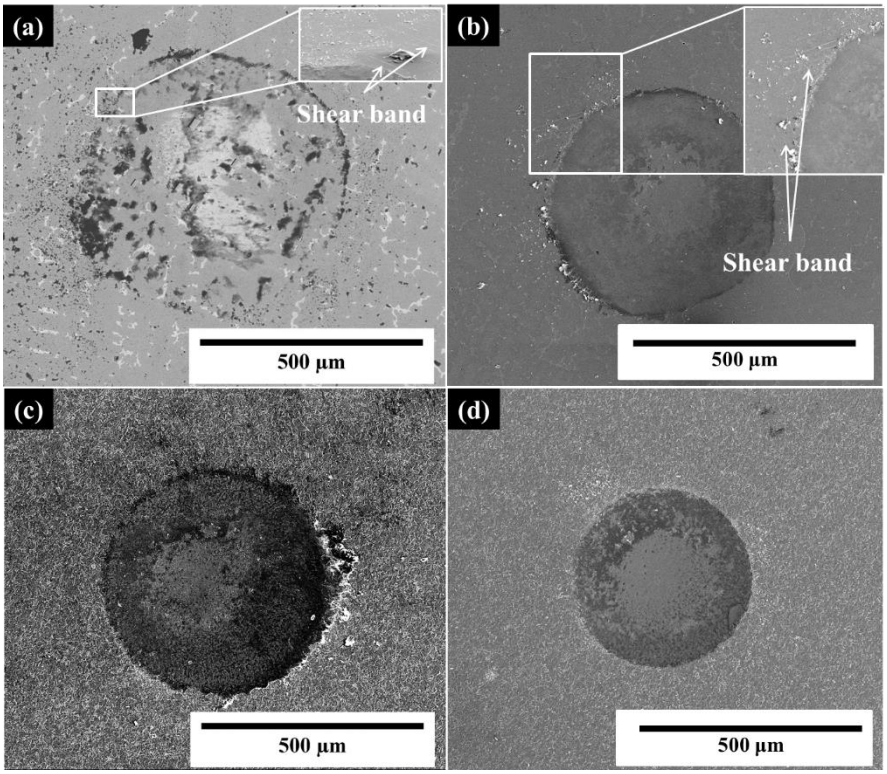

Figure 3

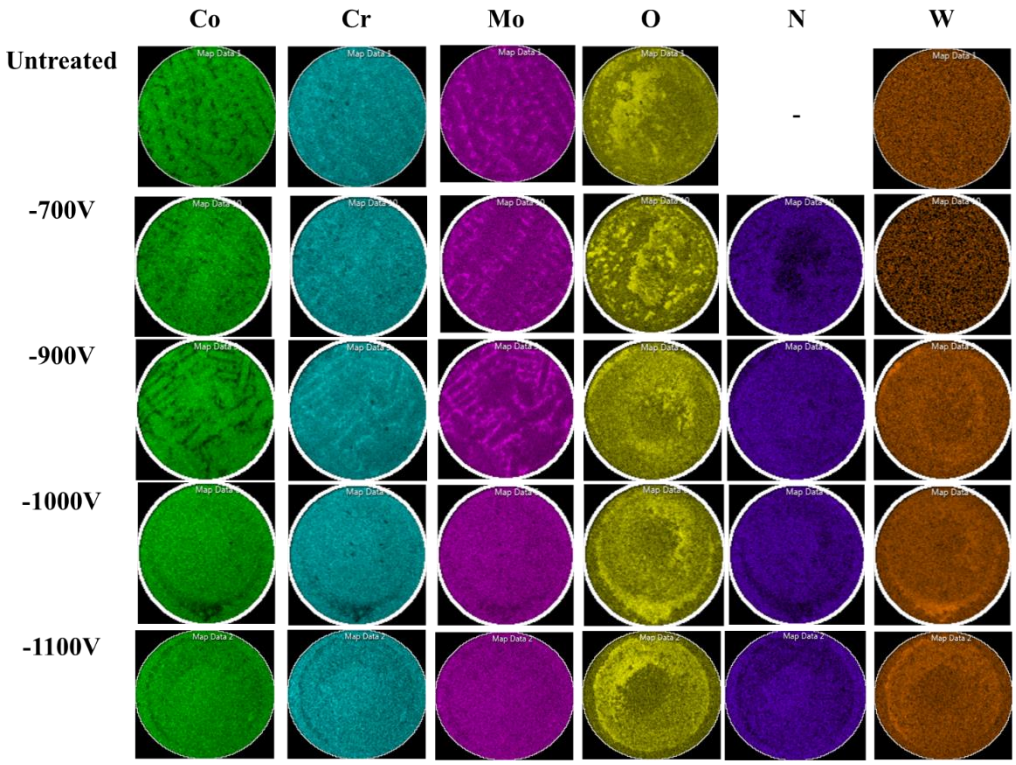

Figure 4

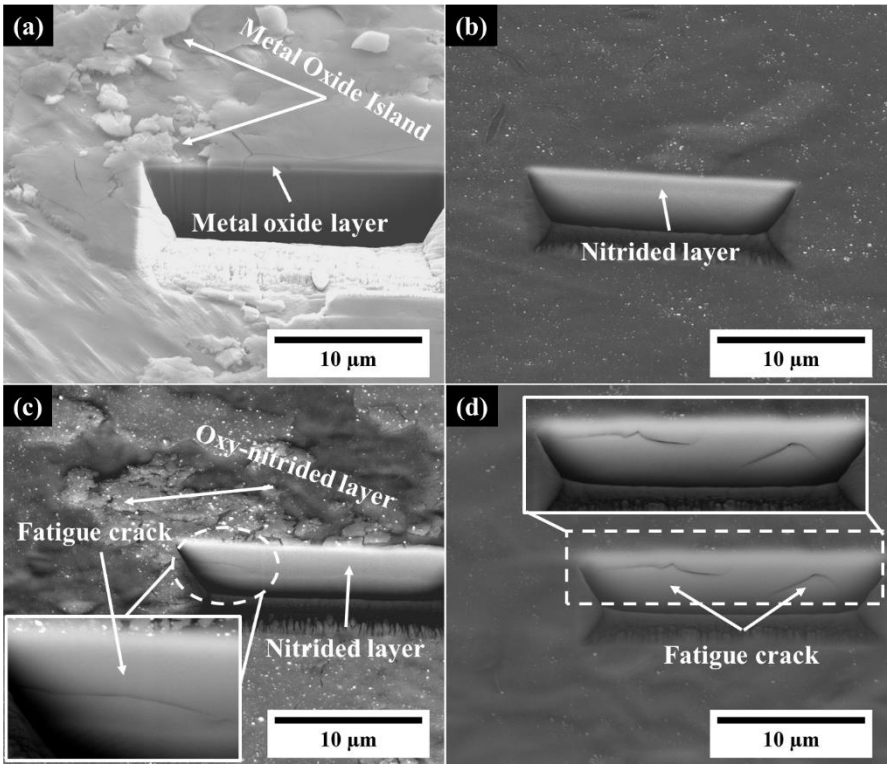

Figure 5

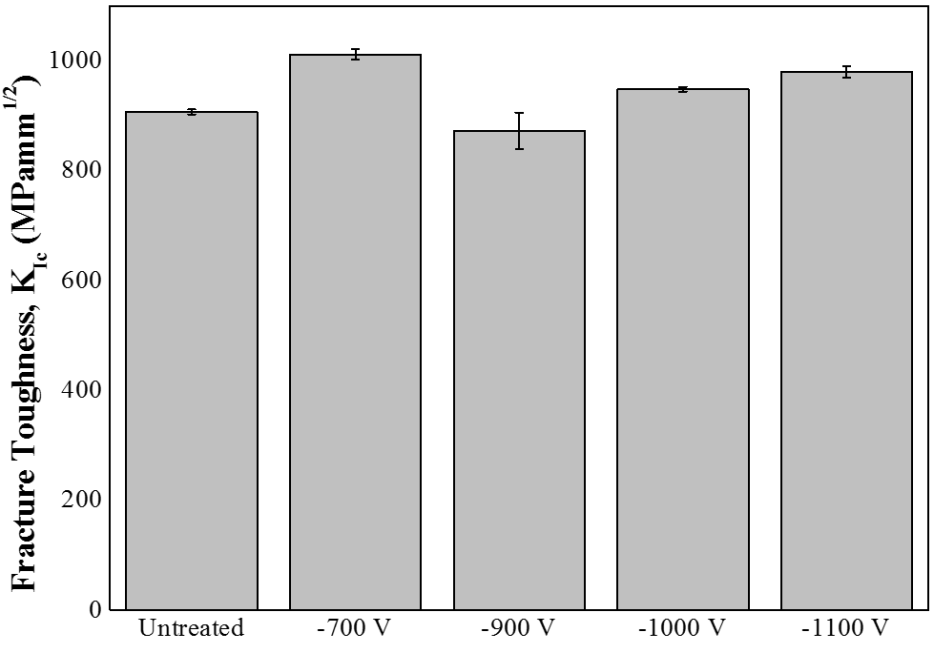
Fracture Toughness, K_{1c} (MPamm$^{1/2}$)
1000
800
600
400
200
0
Untreated
-700 V
-900 V
-1000 V
-1100 V

Figure 6

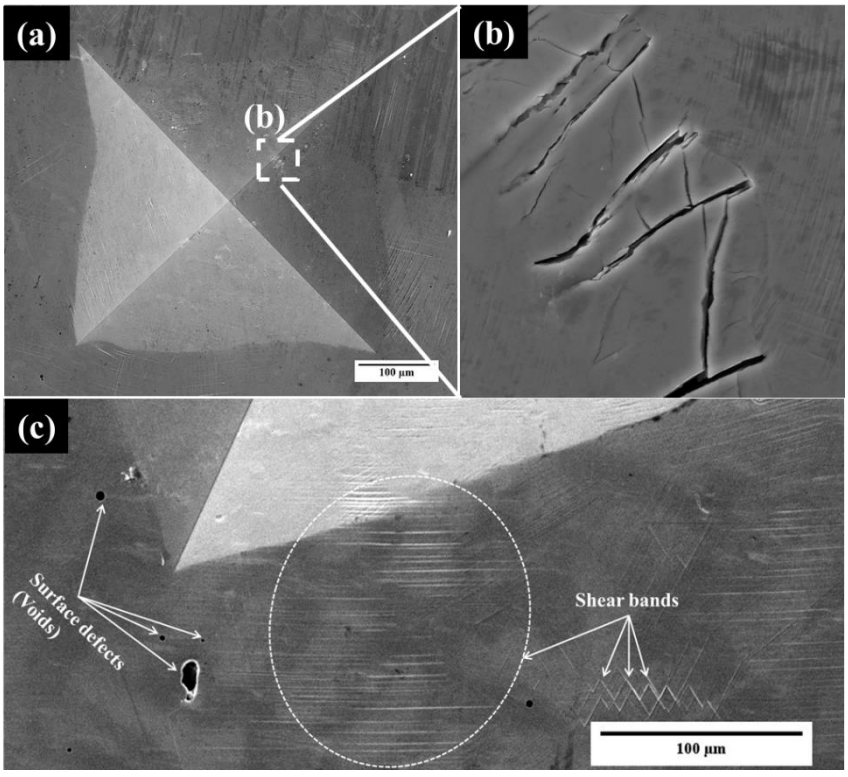
(a)
(b)
100 µm
(b)
(c)
Surface defects
(Voids)
Shear bands
100 µm

Figure 7

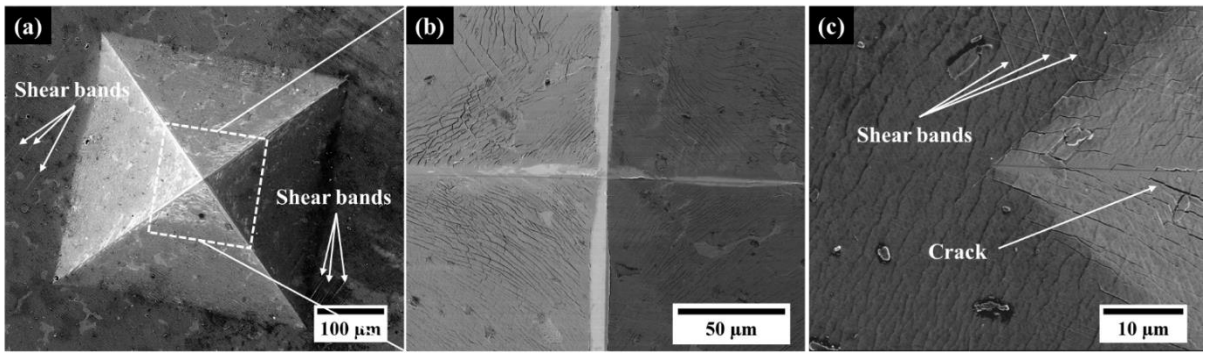

Figure 8

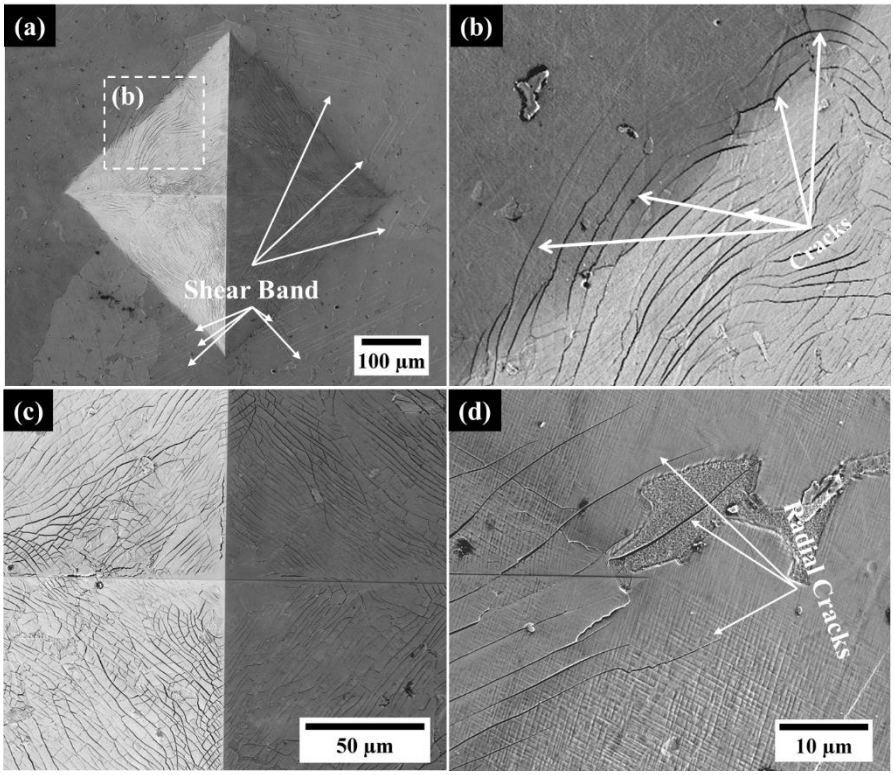

Figure 9

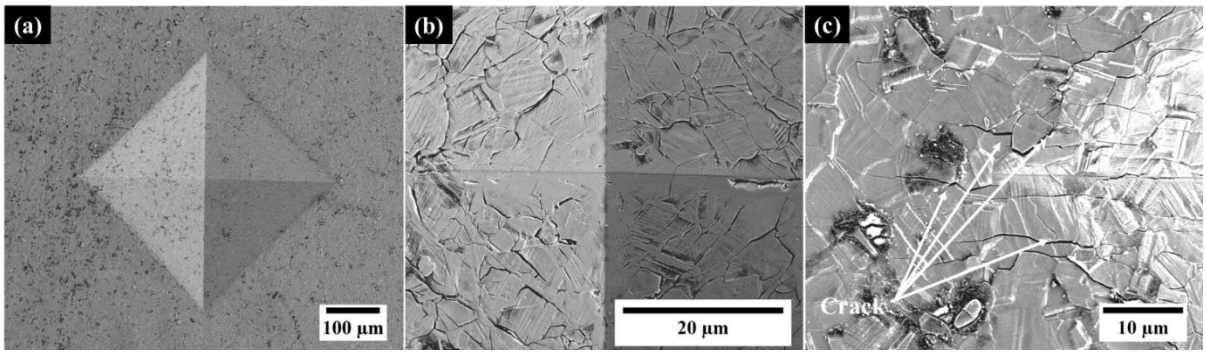

Figure 10

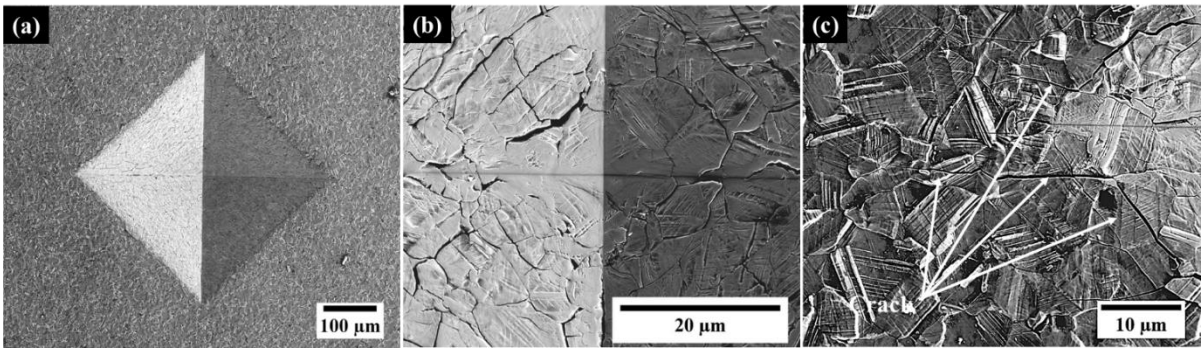

Figure 11

Specimen	Texture (T*)		H (GPa)	E (GPa)	H/E	H^3/E^2	Nitrided layer Thickness (µm)		
	γ_N (111)	γ_N (200)					L_D	L_C	L_T
Untreated	-	-	7.9 ± 0.14	249.4 ± 4.94	0.037	0.008	-	-	-
-700 V	1.51	98.4	22.1 ± 0.67	265.5 ± 4.30	0.083	0.153	0.13	1.10	1.06
-900 V	43.5	56.4	22.98 ±	289.6 ± 3.76	0.078	0.135	0.28	1.32	1.60
-1000 V	33.8	66.1	21.0 ± 1.17	271.6 ± 14.02	0.077	0.126	-	3.62	3.62
-1100 V	28	72	23.0 ± 1.50	343.1 ± 30.91	0.067	0.103		4.91	4.91

Table 1

Specimen Name	Initial Impacts (250), d_i depth (µm)	Final Impact (10^6) depth, d_f (µm)
Untreated	12.73	12.78
-700 V	8.71	11.98
-900 V	9.07	11.34
-1000 V	6.85	7.29
-1100 V	7.16	7.23

Table 2